Aircraft flutter suppression: from a parametric model to robust control

Alex Reis de Souza, C. Poussot-Vassal, Pierre Vuillemin, Jesus Toledo Zucco

HAL Id: hal-04626392

https://hal.science/hal-04626392v1

Submitted on 13 Nov 2024

Aircraft flutter suppression: from a parametric model to robust control

Alex dos Reis de Souza[1,†], Charles Poussot-Vassal[1], Pierre Vuillemin[1], and Jesus Toledo Zucco[1]

Abstract— This paper deals with the suppression of flutter – a type of dynamic instability provoked by the interaction of aerodynamic, inertial, and flexible forces acting over a flexible structure immersed in a fluid – through robust control methods. Since this problem is heavily dependent on flight conditions (such as altitude, speed, etc), an accurate controller synthesis requires a representative model. The Loewner framework offers tools for the generalized realization problem, allowing the construction of such a model using sampled frequency data responses and simple algebraic machinery. This tool helps build a parametric model of an aeroelastic system used then to synthesize a scheduled, dynamic output-feedback robust control law that damps the flexible mode responsible for the appearance of flutter.

I. INTRODUCTION

Flutter is a potentially destructive phenomenon occurring in flexible structured, such as bridges, buildings, or aeronautical structures, when immersed in a fluid flow field. Indeed, it is a self-excited type of instability, characterized by the interaction of inertial, elastic and aerodynamic forces acting in a structure [1].

Focusing on aeronautics, Active Flutter Suppression (AFS) – a topic among many regarding active control technology for aircraft – has been an active field of research over the last decades [2]. AFS algorithms look for controllers that, by actuating over the available control surfaces (such as flaps, ailerons, and elevators), damp the system and avoid flutter of happening in the flight envelope.

In the current literature, this problem is tackled by considering either a 2D airfoil model, or complex models usually obtained through high-fidelity simulators (employing, for instance, finite-element methods). In the first scenario, [3] reviews several adaptive and robust control techniques. Zhang et al. [4] propose an aeroelastic vibration control showing robustness to external gust perturbations, while in [5] a similar result by considering an adaptive, partial state-feedback controller is proposed. Iannelli et al. [6] use the linear robust control framework to analyze the effect of uncertainties on the analysis of flutter.

The second scenario is closer to industrial needs, but imposes several challenges since the models are more complex and often highly dimensional. Nevertheless, interesting results have been obtained notably using robust control. For instance, [7] derive a robust controller through μ-synthesis using an uncertain LTI system, while [8] seeks to ameliorate this controller by constructing a worst-case uncertainty scenario through a multi-frequency gain maximization.

From the perspective of Automatic Control, AFS can be seen as a parametric problem: this phenomenon is dependent on multiple factors, such as the aircraft velocity or its flight altitude (both being linked for a given Mach number). Furthermore, a candidate solution should consist of *(i)* a controller that guarantees stability over the whole flight envelope without disrupting control laws applied to other subsystems of the aircraft (*e.g.*, load alleviation or flight mechanics) and *(ii)* a mechanism coping with the change of flight conditions.

Therefore, it is clear that (parametric) modeling plays a pivotal role in this problem. The Loewner framework (LF) – introduced in [9] – constitutes a data-driven framework for model reduction and identification by interpolation. This technique creates a surrogate model through Lagrange rational interpolation of the available sampled frequency response data. An advantage is that this *interpolant* can be constructed directly from the data set through special matrices: the Loewner and shifted Loewner matrices. In the context of parametric modeling, a very similar LF is employed in this paper, making use of similar Loewner matrix structures [10], [11], [12].

Contribution statement: The contribution of this application-oriented paper is twofold: *(i)* to obtain a parametric reduced-order aeroelastic model prone to flutter through very recent Loewner interpolatory methods, based on aero-servoelastic aircraft data, and *(ii)* using this model, synthesize a robust dynamic controller that aims at preventing the loss of damping of the aircraft. The model, as well as the controller, are parameterized by the flight altitude. By exploiting this parametric dependence, a robust controller verifying all objectives and constraints – typically industrial or certification requirements – can be obtained through state-of-the-art linear control techniques. Furthermore, the used data points follow a format that is standard to aeroelastic engineers, rendering the approach proposed in this paper an end-to-end framework for flutter modeling, analysis and control design.

Notations: The set of real and complex numbers of dimension n are denoted, respectively, by $\mathbb{R}^n$ and $\mathbb{C}^n$. We denote the complex variable $\iota = \sqrt{-1}$. The identity matrix and the null matrix of dimension p read, respectively, I_p and 0_p, while $\mathbf{diag}(\cdot)$ represents a (block) diagonal matrix. The Linear Fractional Transformation (LFT) of blocks M and N are represented by $\mathscr{F}_{l,r}(M,N)$, where the indexes l and r indicate, respectively, a *lower* or an *upper* LFT. The Laplace variable is represented by $s \in \mathbb{C}$ and the parameter vector is

denoted $\theta \in \mathbb{R}^{n_p}$.

Paper organisation: The paper is organised as follows: Section II presents the considered aircraft flutter problem, justifying the use a data-driven methods for the construction of a parametric reduced-order model (pROM), which is carried out through the LF, as detailed in Section III. Then, Section IV uses the pROM to synthesize a flutter controller tackling the performance objectives and constraints. Conclusions and perspectives are given in Section V.

II. THE FLUTTER PROBLEM

A. Parametric aeroelastic flutter model description

The aero-servoelastic (ASE) aircraft model concerned here can be described by the following components: *(i)* the structural part, characterized by the generalized inertia $M(\theta)$, stiffness $K(\theta)$, and damping $D(\theta)$ matrices, *(ii)* an aerodynamic model (representing, for instance, generalized aerodynamic forces) described on the frequency-domain by $Q(s,\theta)$, *(iii)* the sensor locations defined by C and *(iv)* the actuator transfer driven by $B(s,\theta)$.

The (parametric) aeroelastic model coupling the structural and aerodynamic parts is given by:

$$(s^2 M(\theta) + s D(\theta) + K(\theta))x = Q(s,\theta)x + B(s,\theta)u,$$
$$y = Cx, \tag{1}$$

where $\theta \in \mathbb{R}^{n_p}$ is the parameter representing the flight point (*e.g.*, altitude, Mach number, mass), $x \in \mathbb{C}^{n_x}$ is the internal state vector, $u \in \mathbb{C}^{n_u}$ is the input control signal and $y \in \mathbb{C}^{n_y}$ is the available measurement vector. Then, the matrices $M(\theta)$, $D(\theta), K(\theta) \in \mathbb{R}^{n_x \times n_x}$, $Q(s,p) \in \mathbb{C}^{n_x \times n_x}$, $B(s,\theta) \in \mathbb{C}^{n_x \times n_u}$ and $C \in \mathbb{R}^{n_y \times n_x}$. The term $B(s,\theta)$ corresponds to the actuator matrix which, in this work, encompasses the inner and outer ailerons and the elevators (all controlled symmetrically). The term matrix C relates to the measurements, being independent of the flight parameter θ. One important objective of model (1) is to encompass *(i)* the input-output behaviours from actuators to the measurements and *(ii)* to reproduce the stability properties according to the θ parameter value. With this in mind, let us define the flight envelope free of flutter as $\Theta_f = [\underline{\theta}_f, \overline{\theta}_f] \subset \Theta$, where $\underline{\theta}_f < \overline{\theta}_f \in \mathbb{R}^{n_p}$ and Θ is the set containing all the considered flight points.

B. Flutter problem at a glance and considered data

Flutter objective: Considering (1) and the description above, the active flutter control (AFC) problem consists in designing a feedback control law K (not necessarily static) that extends the flutter free domain, *i.e.*, the domain $\Theta_f = [\underline{\theta}_f, \overline{\theta}_f]$ (without control) is smaller than a domain $[\underline{\theta}_f^{(K)}, \overline{\theta}_f^{(K)}]$ (in closed-loop), and is obtained based on a – parametric – dynamical model (see details in Sections III and IV).

Available data and considered set-up: In the set-up considered here, (1) has the following characteristics: $n_x = 89$ internal variables, $n_u = 3$ inputs (the inner and outer ailerons, and elevator) and $n_y = 1$ output (which is the result of an *output blending*, a procedure that optimizes a weighted sum

of three measured quantities – in this work, the pitch rate and two load factors measured on the fuselage – aiming at highlighting the appearance of flutter). Then, the *altitude* is assumed as the single "moving" parameter (see Remark 1), while other parameters are frozen (Mach is set at 0.86 and the mass is set to the half tank configuration).

In addition, the aerodynamic components $Q(s,\theta)$ and $B(s,\theta)$ are known only at few sampled frequency and parameter points, *i.e.*, $Q(\iota\omega_n, \theta_m)$ and $B(\iota\omega_n, \theta_m)$, where $n = 1,\ldots,N = 100$ and $m = 1,\ldots,M = 21$. Note that these values are obtained through dedicated high-fidelity numerical solvers. Similarly, the matrices relating to the structural part – $M(\theta)$, $D(\theta)$, $K(\theta)$ – are also known at frozen parameters values θ_m only, *i.e.*, one has only access to $M(\theta_m), D(\theta_m), K(\theta_m)$.

Grounded in these considerations, the flutter dynamical model allows obtaining data in the frequency-domain. Then, one is able to evaluate (1) at (limited) frozen complex and parametric values $s_n = \iota\omega_n \in \mathbb{C}$ and $\theta_m \in \mathbb{R}$, leading to responses $\Phi_{nm} \in \mathbb{C}^{n_y \times n_u}$. Therefore, the following triplet

$$\{s_n, \theta_m, \Phi_{nm}\}_{n,m=1}^{N,M} \tag{2}$$

constitutes our database and is henceforth simply referred as *data*.

Remark 1: (On pLTI and LPV models): In this work, we consider parametric linear time-invariant (pLTI) models instead of linear parameter-varying (LPV) ones. Indeed, model (1) is only defined in the frequency-domain and for discrete $\{\theta_m\}_{m=1}^M$ values, as explained in (2). As a matter of fact, no information can be retrieved on the dynamics of θ, thus it is mathematically tricky to define such a model as LPV. Therefore, we assume that this parameter is a *slowly varying* one.

III. PARAMETRIC REDUCED ORDER MODELING

A. Identification in the Loewner framework

The LF offers tools for the reduction, approximation, and identification of dynamical systems based on interpolation. It was initially proposed for the non-parametric case in [9], and then extended in the parametric one in [11] (restricted to SISO, SIMO, and MISO systems). Latter, extensions to the (square) MIMO parametric were proposed by [13] and more recently by [12] for general rectangular MIMO systems. In [9], the two-sided LF was introduced, while its one-sided version is preferred in [11], [13], [12] (this point is briefly discussed in this section). A recent overview of the LF is presented by Gosea et al. in [14].

Here, the objective is to use LF tools to build a pROM of an ASE model prone flutter model through the available data (2), obtained from the empirical and partially known model (1). The envisaged pROM must, ideally, match these data and preserve stability (obviously, for configurations that are initially stable). Indeed, the final objective is to use this pROM on the synthesis of a controller that damps the ASE system and suppress flutter.

B. One-sided Loewner: two-variables case

The one-sided two-variables LF version may be employed to construct the pROM based on data (2). From this data, let us consider distinct data subsets $\lambda_i, \mu_k \in \mathbb{C}$ and $\pi_j, \nu_l \in \mathbb{R}$ organised as (where entries of Φ are given by $[\Phi]_{nm}$, $n, m = 1, \ldots, N, M$):

$$
\begin{aligned}
{[s_1, \ldots, s_N]} &= [\lambda_1, \ldots, \lambda_{\overline{n}}] \cup [\mu_1, \ldots, \mu_{\underline{n}}], \\
{[\theta_1, \ldots, \theta_M]} &= [\pi_1, \ldots, \pi_{\overline{m}}] \cup [\nu_1, \ldots, \nu_{\underline{m}}], \\
\Phi &= \left[\begin{array}{c|c} \mathbf{w}_{ij} & \Phi_{12} \\ \hline \Phi_{21} & \mathbf{v}_{kl} \end{array} \right],
\end{aligned} \tag{3}
$$

for which one seeks $\mathbf{H}(s, \theta) = C(\theta)(sE - A(\theta))^{-1}B(\theta)$ such that

$$
\begin{aligned}
\mathbf{H}(\lambda_i, \pi_j) &= \mathbf{w}_{ij} \quad i = 1 \ldots \overline{n} \text{ and } j = 1, \ldots, \overline{m}, \\
\mathbf{H}(\mu_k, \nu_l) &= \mathbf{v}_{kl} \quad k = 1 \ldots \underline{n} \text{ and } l = 1, \ldots, \underline{m}.
\end{aligned} \tag{4}
$$

Remark 2 (Data partitioning): Throughout this section, let $\overline{n} - 1$ and $\overline{m} - 1$ define the order of rational approximation of the model $\mathbf{H}(s, \theta)$ along s and θ, respectively. Interested reader may refer to [11], [12] and to the recent overview [14] for further details.

To construct a realization $\Sigma(\theta)$ of the transfer $\mathbf{H}(s, \theta)$ that ensures (4), one constructs the *one-sided, two-variables Loewner matrix* given by

$$
\widehat{\mathbb{L}}_2 = \begin{bmatrix} \mathbb{L}_2^\top & \mathbb{L}_\lambda^\top & \mathbb{L}_\pi^\top \end{bmatrix}^\top, \tag{5}
$$

where

$$
\begin{aligned}
{[\mathbb{L}_2]_{i,j}^{k,l}} &= \frac{\mathbf{v}_{kl} - \mathbf{w}_{ij}}{(\mu_k - \lambda_i)(\nu_l - \pi_j)}, \\
\mathbb{L}_\lambda &= \mathbf{diag}(\mathbb{L}_{\lambda_1}, \ldots, \mathbb{L}_{\lambda_{\overline{n}}}), \\
\mathbb{L}_\pi &= \left[\mathbf{diag}\big(\mathbb{L}_{\pi_1}(:,1), \ldots, \mathbb{L}_{\pi_{\overline{m}}}(:,1)\big), \ldots, \right. \\
&\quad \left. \mathbf{diag}\big(\mathbb{L}_{\pi_1}(:,\overline{n}), \ldots, \mathbb{L}_{\pi_{\overline{m}}}(:,\overline{n})\big) \right],
\end{aligned} \tag{6}
$$

where $[\mathbb{L}_{\lambda_i}]$ is the one variable Loewner of the i-th row of Φ, interpolating at nodes (λ_i, ν_d) (for $d = 1, \ldots, \underline{m}$):

$$
[\mathbb{L}_{\lambda_i}] = \begin{bmatrix} \frac{\Phi_{i,\overline{m}+1} - \mathbf{w}_{i,1}}{\nu_1 - \pi_1} & \cdots & \frac{\Phi_{i,\overline{m}+1} - \mathbf{w}_{i,\overline{m}}}{\nu_1 - \pi_{\overline{m}}} \\ \vdots & \ddots & \vdots \\ \frac{\Phi_{i,M} - \mathbf{w}_{i,1}}{\nu_{\underline{m}} - \pi_1} & \cdots & \frac{\Phi_{i,M} - \mathbf{w}_{i,\overline{m}}}{\nu_{\underline{m}} - \pi_{\overline{m}}} \end{bmatrix} \tag{7}
$$

and where $[\mathbb{L}_{\pi_j}]$ is the *one variable* Loewner of the j-th column of Φ, interpolating at nodes (μ_t, π_j) (for $t = 1, \ldots, \underline{n}$):

$$
[\mathbb{L}_{\pi_j}] = \begin{bmatrix} \frac{\Phi_{\overline{n}+1,j} - \mathbf{w}_{1,j}}{\mu_1 - \lambda_1} & \cdots & \frac{\Phi_{\overline{n}+1,j} - \mathbf{w}_{\overline{n},j}}{\mu_1 - \lambda_{\overline{n}}} \\ \vdots & \ddots & \vdots \\ \frac{\Phi_{N,j} - \mathbf{w}_{1,j}}{\mu_{\underline{n}} - \lambda_1} & \cdots & \frac{\Phi_{N,j} - \mathbf{w}_{\overline{n},j}}{\mu_{\underline{n}} - \lambda_{\overline{n}}} \end{bmatrix} \tag{8}
$$

According to [11], [12], by choosing $r+1 = \overline{n}$ and $q+1 = \overline{m}$, (5) satisfies $\mathbf{rank}(\widehat{\mathbb{L}}_2) = \mathbf{rank}(\mathbb{L}_2) = \overline{n}\overline{m} - (\overline{n} - N)(\overline{m} - M)$. Then, solving $\widehat{\mathbb{L}}_2 \mathbf{c} = 0$ for $\mathbf{c} \neq 0$ leads to the Barycentric rational interpolating function

$$
\mathbf{H}(s, \theta) = \frac{\sum_{i=1}^{r+1} \sum_{j=1}^{q+1} \frac{\mathbf{c}_{ij} \mathbf{w}_{ij}}{(s - \lambda_i)(\theta - \pi_j)}}{\sum_{i=1}^{r+1} \sum_{j=1}^{q+1} \frac{\mathbf{c}_{ij}}{(s - \lambda_i)(\theta - \pi_j)}}, \tag{9}
$$

satisfying (4). From (9) and using the Lagrangian basis presented in [10], one may construct a representation of $\mathbf{H}(s, \theta)$ given by a parametric state-space realization of dimension $r + \min(n_u, n_y)$,

$$
\Sigma(\theta) : \left(E, A + \sum_{k=1}^q A_i \theta^q, B + \sum_{i=1}^q B_i \theta^q, C, 0 \right). \tag{10}
$$

Remark 3: (About q and r): Orders q and r are defined by the designer. In practice, one may apply the single-valued Loewner rank revealing factorization for each Loewner $\mathbb{L}_{\lambda_i}$ and $\mathbb{L}_{\pi_j}$ matrices and chose the maximum order along $\mathbb{L}_{\lambda_i}$ for q and $\mathbb{L}_{\pi_j}$ for r (see [11]).

Remark 4: (About the one-sided single-variable LF): In the non-parametric case (or *single-variable case*) θ_m is a singleton, *i.e.*, $M = 1$ in (2). In this case, one constructs the *one-sided Loewner matrix* $\mathbb{L}_1$ as

$$
[\mathbb{L}_1]_{ik} = \frac{\mathbf{v}_k - \mathbf{w}_i}{\mu_k - \lambda_i} \in \mathbb{C}^{n_y \times n_u}. \tag{11}
$$

Solving $\mathbb{L}_1 \mathbf{c} = 0$ for non-trivial $\mathbf{c}$ leads to (the non-minimal) rational function $\mathbf{H}(s)$, which may be expressed in the Lagrangian basis as $(r + 1 = \overline{n})$

$$
\mathbf{H}(s) = \frac{\sum_{i=1}^{r+1} \frac{\mathbf{c}_i \mathbf{w}_i}{(s - \lambda_i)}}{\sum_{i=1}^{r+1} \frac{\mathbf{c}_i}{(s - \lambda_i)}}. \tag{12}
$$

In this case, the rth order rational function $\mathbf{H}(s)$, equipped with a realisation of order $r + \min(n_u, n_y)$, interpolates the available data. The interested reader may refer to [10], [13] for more details.

Remark 5: (About the two-sided single-variable (tangential) LF): In the two-sided single-variable case, the main difference is the apparition of a Loewner (as in $\mathbb{L}_1$) together with a shifted Loewner matrix denoted $\mathbb{M}_1$. Both $\mathbb{L}_1, \mathbb{M}_1$ constitute the Loewner pencil. Without loss of generality and referring to [9], we show that $\mathbf{H}(s) = \mathbf{W}(-s\mathbb{L}_1 + \mathbb{M}_1)^{-1}\mathbf{V}$ (tangentially) interpolates the data ($\mathbf{W}$ and $\mathbf{V}$ being given by the data partitioning $\mathbf{w}_i$ and $\mathbf{v}_k$). In addition, if the data have been generated by a linear model, the rational order $r = \mathbf{rank}(s\mathbb{L}_1 - \mathbb{M}_1) = \mathbf{rank}([\mathbb{L}_1, \mathbb{M}_1]) = \mathbf{rank}([\mathbb{L}_1^H, \mathbb{M}_1^H]^H)$ recovers the one of the generating system, as well as its McMillan degree ν is given by $\nu = \mathbf{rank}(\mathbb{L}_1)$. It is assumed that enough data is available. In conclusion, the two-sided LF allows the approximation and identification based on frequency reponses, while also encoding fundamental realisation-oriented properties, *e.g.*, the McMillan degree and the minimal realisation order [14], [15]. However, this is not true for the parametric case, where this point stands as an open problem.

C. Application on the flutter use-case

Applying the LF tools described above to the problem stated in Section II, one obtains a pROM describing system (1) with a rational order $r = 30$ and with a (rational) parameter dimension $q = 1$. The parameter $\theta \in \mathbb{R}^q$ represents the flight altitude. The state-space realization, which has an order $n_x = 31$, reads

$$
\Sigma(\theta) : (E, A + A_1 \theta, B + B_1 \theta, C, 0). \tag{13}
$$
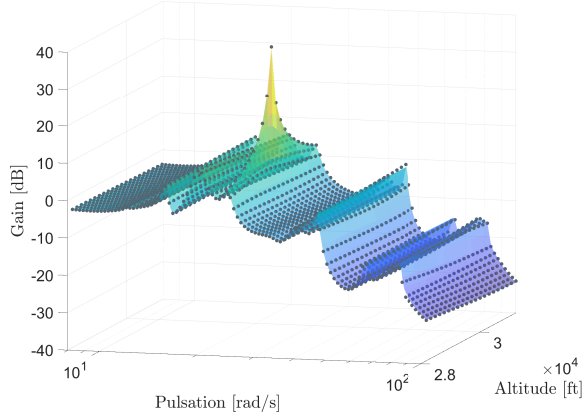
Fig. 1. Frequency sigma plot for varying altitudes. Original data (2) (grey dots) and interpolated model $\mathbf{H}(s,\theta)$ of order $k=30, q=1$ (orange lines).
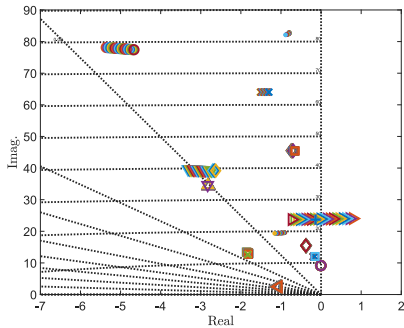
Fig. 2. Eigenvalues for varying altitudes of the interpolated model $\mathbf{H}(s,\theta)$ of order $k=30$, $q=1$ (orange dots). The flutter dynamic is mainly governed by the right triangle eigenvalues.

The data along s_n are logarithmically spaced between $\iota 10$ and $\iota 100$, with $N = 100$. For the parameter θ, which is enclosed in the interval $\theta \in \Theta = [2.82,\ 3.12] \times 10^4$ ft, the available data is linearly spaced in such an interval with $M = 21$.

Instability, caused by the loss of damping, can be observed for all $\theta \le \underline{\theta}_f = 2.95 \times 10^4$ ft. Fig. 1 depicts the evolution of the singular values of $\mathbf{H}(s,\theta)$, also highlighting the appearance of a resonant peak in a frequency range $\omega \in [23, 25]$ rad/s.

In complement, Fig. 2 shows the eigenvalues of the pROM as a function of the parameter θ. One notices that the crossing of the imaginary axis happens in the same frequency range, evidencing that such a peak represents the frontier between unstable/stable eigenvalues. This point plays an important role in the control design, as it will be discussed in the next section.

IV. OUTPUT-FEEDBACK ROBUST CONTROLLER

This section aims at designing a robust controller exploiting the pROM obtained in the previous section. The control problem will be tackled considering the block scheme shown in Fig. 3. Although seemingly unusual, this configuration takes δ_u as the *pilot command to the control surfaces* – command which is taken into account together with the
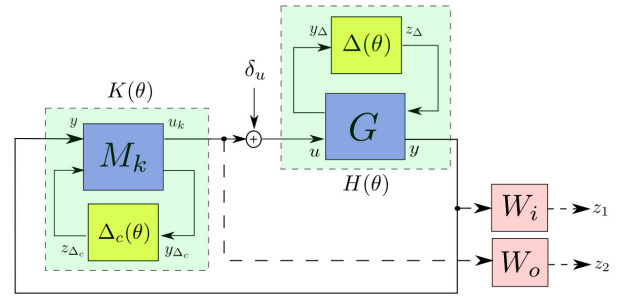
Fig. 3. Illustration of the implemented control block scheme. Here, G and M_k are nominal systems, while $\Delta(\theta)$) and $\Delta(\theta)$ represent their uncertainty blocks. The signals y_Δ and z_Δ are internal and relate to the link the nominal and the uncertain blocks.

(internal) stabilizing signal computed by controller K. This controller must endow the closed-loop system with the following features:

(C1) It must extend the stability envelope defined by $P(\theta)$, without deteriorating stability of the points that are already stable;

(C2) It must not change the low-frequency behaviour of the aircraft (since it relates to its flight mechanics and maneuverability);

(C3) It must be stable and have roll-off characteristics (to avoid the excitation of high-frequency modes).

Since a controller with a fixed structure is envisaged, this section will use the structured $\mathscr{H}_\infty$ synthesis proposed by [16], implemented in Matlab as the routine `hinfstruct`, whereas the computation of the structured singular values is carried out using the SMART library of the SMAC toolbox [17].

A. Robust controller design

Considering the scheme shown in Fig. 3, let

$$P(\theta) : W_o(s)\mathbf{H}(s,\theta)W_i(s)$$

denote the generalized plant containing the uncertain plant (*i.e.*, the pROM) plus input/output performance weighting functions $W_o(s)$ and $W_i(s)$.

According to the objective of attenuating the resonating peak, $W_o(s)$ is a performance filter relating to the $\mathscr{H}_\infty$ norm (or, equivalently, the peak shown in Fig. 1), *i.e.*, $W_o(s) = \|T_{yu}\|_\infty^{-1}$, whereas $W_i(s)$ relates to the dynamic behavior of the controller. Notably, in order to respect the requirements (C2) and (C3), this performance filter should have roll-off and a low-frequency gains.

The controller proposed in this paper is a *parametric, dynamic, output-feedback* one, being described by the following matrices:

$$K(\theta) : \begin{cases} \dot{x}_c &= A_c(\theta)x_c + B_c(\theta)y \\ u &= C_c(\theta)x_c \end{cases} \tag{14}$$

where $A_c(\theta) \in \mathbb{R}^{n_c \times n_c}$, $B_c(\theta) \in \mathbb{R}^{n_c \times n_y}$, and $C_c(\theta) \in \mathbb{R}^{n_u \times n_c}$ are the matrices to be determined. This controller – which is

scheduled regarding the altitude, *i.e.*, parameter θ – can be obtained through the solution of the following optimization problem:

$$K(\theta) = \arg \min_{\substack{K \in \mathscr{K} \\ \theta \in \Theta}} \gamma, \qquad (15)$$

where

$$\gamma = \|\mathscr{F}_l(P(\theta), K(\theta))\|_\infty. \qquad (16)$$

The set $\mathscr{K} \subseteq \mathscr{H}_2$ represents the set of all controllers with the desired structured given by (14). Under this constraint, K will be restricted to such a structure, while automatically fulfilling the stability requirement imposed by (C3).

Remark 6: Note that one can further structure controller (14) by defining the parameter-dependent matrices as affine (*e.g.*, $A_c(\theta) = A_{c,0} + A_{c,1}\theta$). In this form, the controller can be easily rewritten as an LFT, as initially depicted in Fig. 3.

Design through a multi-model approach: An option for robust synthesis is the *multi-model approach*, which consists in concatenating several constraints into a single transfer matrix when solving (15). Each constraint might relate, for instance, to different requirements or even different plants sampled w.r.t. θ, *i.e.*, (16) becomes

$$H = \mathbf{diag}(H_1, \ldots, H_n)$$

where each H_i can be rewritten on the form $\mathscr{F}_l(P(\theta_i), K(\theta_i))$. Note that, in such a scenario, different performance filters might be used. The solution of (15) will represent the worst-case $\mathscr{H}_\infty$ norm over all these generalized constraints.

However, due to this sampling over θ, no *robust stability* certificate can be directly obtained from this synthesis. Nevertheless, an interesting way out is to use μ-analysis *a posteriori* to analyze the robust performance of the obtained closed-loop, *i.e.*, to infer how robust it is regarding possible variations of considered the uncertainty.

B. Synthesis and evaluation of the controller

Following the discussion presented in the previous subsection, we select $n_c = 4$ and the performance filter for the control signal as

$$W_i(s) = G_{lp}(s)G_{pb}(s),$$

$$G_{lp} = k_{lp}\left(\frac{k_{lp}/\omega_0 s + 1}{1/\omega_0 s + 1}\right)^2, \quad G_{pb} = \frac{s^2/k_2 + k_3\omega_c + \omega_c^2}{s^2 + k_3\omega_c s + \omega_c^2}$$

Note that G_{lp} and G_{pb} are, respectively, a high-pass and band-pass filter. Their parameters are chosen as $k_{lp} = 50$, $\omega_0 = 10$ rad/s, $\omega_c = 25$ rad/s, $k_2 = 0.025$, and $k_3 = 4$. With this filter, one penalizes the influence of the controller in frequencies below 10 rad/s, while enhancing its influence around 25 rad/s.

We sample 6 linearly spaced values of $\theta \leq \theta_f$ (*i.e.*, among the unstable flight points) in order to build the generalized constraints. The solution of (15) with `hinfstruct` returns $\gamma = 0.418$, taking approximately 1 hour of execution. The controller obtained is depicted (in terms of its singular values) in Fig. 4, along with the inverse of the performance
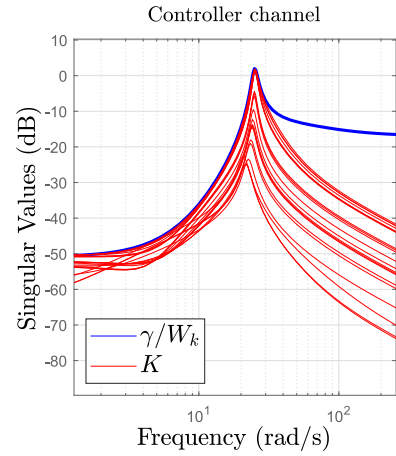
Fig. 4. Controller template (W_k) used for the synthesis (blue), singular values of the obtained controller for different θ (orange).

filter W_i weighted by γ. Conclusively, one has that, for any realization of θ, *(i)* the worst-case transfer respects the imposed template, and *(ii)* the controller is stable.

Performing the μ-analysis on the resulting closed-loop, one obtains $\mu \in [0.5699, 0.9390]$. According to [17], since the structured singular values are below one, this loop is robustly stable w.r.t the structured uncertainties considered. This means that the ASE remains stable for any $\theta \in \Theta$, representing an extension of the flight envelope (regarding the altitude and for the fixed Mach number) by around 1.51×10^3 ft.

The effectiveness of the flutter-suppressing controller can also be evaluated through Figs. 5 and 6. Fig. 5 shows that the resonant peak is attenuated by roughly 30dB, while keeping the lower frequency transfers untouched. Fig. 6 illustrates the increasing of the (minimum and flutter-related) damping ratio in both open- and closed-loop configurations.

Finally, Fig. 7 illustrates the pole-zero map for both configurations. As it can be seen, the controller enhances the damping of the poles related to flutter, moving them away from the imaginary axis. It is worth noticing that the controller does not touch the poles in lower frequencies, as imposed by requirement (C1).

V. CONCLUSIONS & PERSPECTIVES

In this paper, we have presented a complete end-to-end methodology for the construction of a parametric aeroelastic model, which is then used for the design of a robust controller aiming at flutter suppression. The methodology is illustrated using data from a case study of an aeronautical industry. Since this data has a standard format as used by aeroelastic engineers, the proposed methodology is readily applicable to real-life applications.

The parametric model was constructed through the Loewner framework, a data-driven and computationally inexpensive tool for reduction and identification. The robust controller – synthesized through a multi-model $\mathscr{H}_\infty$ approach – is scheduled w.r.t flight altitude and helps to damp the
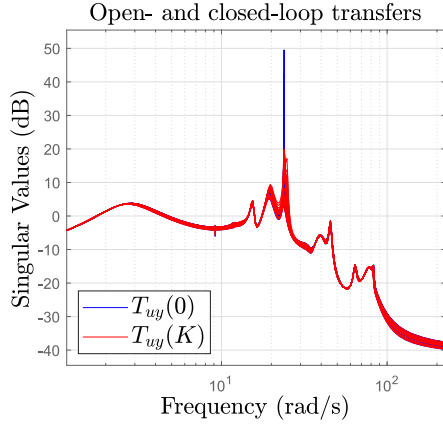
Fig. 5. Open- and closed-loop transfers $T_{uy} : \delta_u \mapsto y$, for all realizations of θ. The zooming box highlights the frequency range which should not be touched by the controller.
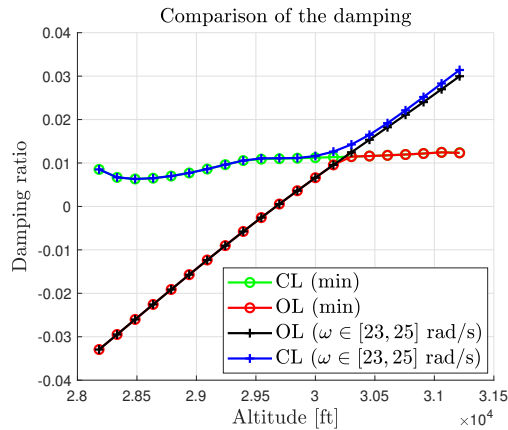
Fig. 6. Evolution of the damping w.r.t. the altitude.
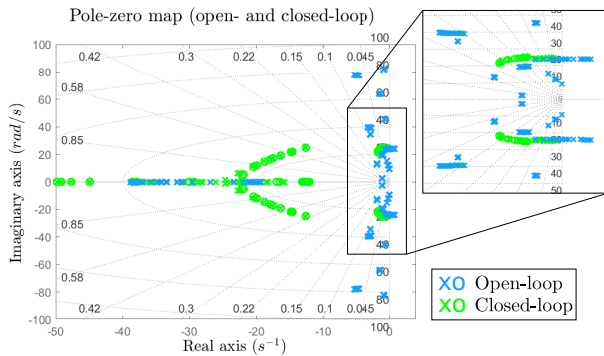
Fig. 7. Pole locations in open- and closed-loop. The poles the migrate to the right half-plane are the ones relating to the flutter.

system for lower altitudes (and, therefore, avoiding flutter and extending the flight envelope), while also avoiding any detrimental effect on lower frequencies. Robust stability is assessed by means of a μ-analysis of the closed-loop.

Future directions of research include *(i)* study a realization containing the Mach number as a parameter (allowing the controller synthesis to comprehend several iso-Mach lines), and *(ii)* enhancing the synthesis with better constraints and considering further uncertainties (such as measurement noise and delay). A study on control saturation is also envisaged.

REFERENCES

[1] T. Theodorsen and I. Garrick, "Mechanism of flutter a theoretical and experimental investigation of the flutter problem," tech. rep., National Aeronautics and Space Administration, Washington D.C., 1940.
[2] E. Livne, "Aircraft active flutter suppression: State of the art and technology maturation needs," *Journal of Aircraft*, vol. 55, no. 1, pp. 410–452, 2018.
[3] W. Z., B. A., and M. P., "Adaptive and robust aeroelastic control of nonlinear lifting surfaces with single/multiple control surfaces: A review," *International Journal of Aeronautical and Space Sciences.*, 2010. https://doi.org/10.5139/ijass.2010.11.4.285.
[4] K. Zhang and A. Behal, "Continuous robust control for aeroelastic vibration control of a 2-d airfoil under unsteady flow," *Journal of Vibration and Control*, vol. 22, no. 12, pp. 2841–2860, 2016.
[5] K. Zhang, Z. Wang, A. Behal, and P. Marzocca, "Novel nonlinear control design for a two-dimensional airfoil under unsteady flow," *Journal of Guidance, Control, and Dynamics*, vol. 36, no. 6, pp. 1681–1694, 2013.
[6] A. Iannelli, A. Marcos, and M. Lowenberg, "Aeroelastic modeling and stability analysis: A robust approach to the flutter problem," *International Journal of Robust and Nonlinear Control*, vol. 28, no. 1, pp. 342–364, 2018.
[7] B. Patartics, G. Lipták, T. Luspay, P. Seiler, B. Takarics, and B. Vanek, "Application of structured robust synthesis for flexible aircraft flutter suppression," *IEEE Transactions on Control Systems Technology*, vol. 30, no. 1, pp. 311–325, 2022.
[8] B. Patartics, P. Seiler, B. Takarics, and B. Vanek, "Worst case uncertainty construction via multifrequency gain maximization with application to flutter control," *IEEE Transactions on Control Systems Technology*, pp. 1–11, 2022.
[9] A. Mayo and A. Antoulas, "A framework for the solution of the generalized realization problem," *Linear Algebra and its Applications*, vol. 425, no. 2, pp. 634–662, 2007. Special Issue in honor of Paul Fuhrmann.
[10] A. Antoulas, A. Ionita, and S. Lefteriu, "On two-variable rational interpolation," *Linear Algebra and its Applications*, vol. 436, pp. 2889–2915, April 2012.
[11] A. Ionita and A. Antoulas, "Data-Driven Parametrized Model Reduction in the Loewner Framework," *SIAM Journal on Scientific Computing*, vol. 36, no. 3, pp. A984–A1007, 2014.
[12] T. Vojkovic, D. Quero, C. Poussot-Vassal, and P. Vuillemin, "Low-order parametric state-space modeling of MIMO systems in the Loewner framework," *SIADS*, submitted.
[13] S. Lefteriu, A. Antoulas, and A. Ionita, "Parametric model reduction in the loewner framework," *IFAC Proceedings Volumes*, vol. 44, no. 1, pp. 12751–12756, 2011. 18th IFAC World Congress.
[14] I. Gosea, C. Poussot-Vassal, and A. Antoulas, "Data-driven modeling and control of large-scale dynamical systems in the Loewner framework," *Handbook of Numerical Analysis*, vol. 23, no. Numerical Control: Part A, pp. 499–530, 2022.
[15] I. Gosea and A. Antoulas, "The One-Sided Loewner Framework and Connections to Other Model Reduction Methods Based on Interpolation," in *Proceedings of the 25th International Symposium on Mathematical Theory of Networks and Systems*, (Bayreuth, Germany), September 2022.
[16] P. Apkarian and D. Noll, "Nonsmooth $\mathcal{H}_\infty$ synthesis," *IEEE Transactions on Automatic Control*, vol. 51, no. 1, pp. 71–86, 2006.
[17] J.-M. Biannic, L. Burlion, F. Demourant, G. Ferreres, G. Hardier, T. Loquen, and C. Roos, "The SMAC Toolbox: a collection of libraries for Systems Modeling, Analysis and Control," June 2016.